



**HAL**  
open science

# New directional wave satellite observations: Towards improved wave forecasts and climate description in Southern Ocean

Lotfi Aouf, Danièle Hauser, Chapron Bertrand, A. Toffoli, C. Tourrain, C. Peureux

## ► To cite this version:

Lotfi Aouf, Danièle Hauser, Chapron Bertrand, A. Toffoli, C. Tourrain, et al.. New directional wave satellite observations: Towards improved wave forecasts and climate description in Southern Ocean. Geophysical Research Letters, In press, Geophysical Research Letters, pp.10.1029/2020GL091187. insu-03008401v1

**HAL Id: insu-03008401**

**<https://insu.hal.science/insu-03008401v1>**

Submitted on 16 Nov 2020 (v1), last revised 15 Jun 2021 (v3)

**HAL** is a multi-disciplinary open access archive for the deposit and dissemination of scientific research documents, whether they are published or not. The documents may come from teaching and research institutions in France or abroad, or from public or private research centers.

L'archive ouverte pluridisciplinaire **HAL**, est destinée au dépôt et à la diffusion de documents scientifiques de niveau recherche, publiés ou non, émanant des établissements d'enseignement et de recherche français ou étrangers, des laboratoires publics ou privés.

1  
2  
3  
4  
5  
6  
7  
8  
9  
10  
11  
12  
13  
14  
15  
16  
17  
18  
19  
20  
21  
22  
23  
24  
25

**New directional wave satellite observations : Towards improved wave forecasts and climate description in Southern Ocean**

**L. Aouf<sup>1</sup>, D. Hauser<sup>2</sup>, B. Chapron<sup>3</sup>, A. Toffoli<sup>4</sup>, C. Tourrain<sup>5</sup>, C. Peureux<sup>6</sup>**

<sup>1</sup>Météo-France, CNRM-DirOP, Toulouse, France

<sup>2</sup>LATMOS/IPSL, Guyancourt, France

<sup>3</sup>IFREMER, Brest, France

<sup>4</sup>University of Melbourne, Melbourne, Australia

<sup>5</sup>CNES, Toulouse, France

<sup>6</sup>CLS, Brest, France

Corresponding author: Lotfi Aouf (lotfi.aouf@meteo.fr)

†Current address : Météo-France, DirOP/MAR, 42 Avenue Gaspard Coriolis Toulouse 31057 Cedex 1, France..

**Key Points:**

- The assimilation of partitions wavenumber components induces a significant reduction of SWH bias in Southern Ocean.
- The study clearly reveals the improvement of the energy transfer of wind waves during the wave growth phase under unlimited fetch conditions such in Pacific Southern Ocean.
- The wave age and dominant wavenumber have been significantly corrected by the assimilation of directional observations of SWIM compared to the assimilation of SWH-nadir only.

## 26 **Abstract**

27 In spite of continuous improvements of ocean wave models in the last decades, results still show  
28 large in certain condition, in particular in strongly forced conditions, as encountered in the  
29 Southern Ocean, where strong westerly winds generate some of the fiercest waves on Earth in  
30 almost unlimited fetch conditions. The newly launched Chinese-French Oceanography Satellite  
31 (CFOSAT) provides directional spectra of ocean waves for both wind seas and swells. Compared  
32 to Synthetic Aperture Radar (SAR), it resolves shorter wavelengths, which dominates in non-  
33 fully developed wind waves. Here we demonstrate that the assimilation of the wave number  
34 components from CFOSAT spectra produce more accurate predictions of wave growth than  
35 assimilation of significant wave height alone and results in a notable reduction of model bias in  
36 the Southern Ocean, especially in the Pacific Ocean sector. In addition results also indicate a  
37 downward shift of the wave age consistent with theoretical wave growth curves.

38

## 39 **Plain Language Summary**

40

41 This work focuses on the importance of using directional wave observations to improve model  
42 wave prediction in the Southern Ocean. The results indicate a significant impact on the transition  
43 from a wind-dependent sea to a well-developed sea. A direct consequence of this work will  
44 concern a better understanding of the wave climate in Southern Ocean and therefore an  
45 improvement of coupled ocean/waves/atmosphere systems.

46

## 47 **1 Introduction**

48 The accuracy of wave prediction models has increased notably over the past decade, following  
49 the improvement of atmospheric models, which provide the wind forcing. Furthermore,  
50 development of assimilation techniques has allowed the incorporation of satellite data into  
51 models to optimize performances (Lionello et al, 1992). In this respect, space-borne altimeter  
52 sensors scan the ocean surface globally and return observations of significant wave height—a  
53 measure of the overall energy content of the wavy surface—which contributes to adjusting the  
54 variance of the wave energy spectrum. Moreover, Synthetic Aperture Radar (SAR) technology  
55 provides images that can be converted into directional wave energy spectra. Assimilation of the  
56 latter enables a more comprehensive control of the energy density function, not only allowing the  
57 optimization of the variance, but also controlling wave periods and wave directions for example  
58 (Aouf et al, 2019). Nevertheless, SAR only detects swell systems, i.e. a long wave system no  
59 longer under the effect of local wind, with wavelength longer than 200 m (Collard et al. 2005),  
60 but does not resolve, and thus assimilation does not correct, the wind sea, i.e. the short-wave  
61 components directly generated by the local wind.

62 Generation and growth of wind sea depend on the fetch conditions (Hasselmann et al, 1973,  
63 Donelan et al, 1985, Young 1999), and generate (nonlinear) energy transfer across wave scales  
64 until an equilibrium state (full development) is reached. More specifically, the transfer consists  
65 of an inverse cascade transferring energy from high to low frequencies, which downshifts the  
66 spectral peak, stretches the wavelengths and consequently accelerates the wave phase speed.

67 Growth stops, and wind sea becomes swell, when the ratio of the wave phase speed to the wind  
68 speed (i.e. wave age) is greater than about 1.2 (atmosphere cannot force waves that move faster  
69 than the wind, Pierson and Moskowitz 1964, Phillips 1977, Hasselmann et al. 1973, Young  
70 1999). Concomitantly, there is a direct cascade that shifts energy towards high frequencies,  
71 forcing energy to dissipate mostly by wave breaking and counterbalancing wind input.

72 Energy further re-distributes across directions so that the wave spectrum broadens during growth  
73 (e.g. Hasselmann et al , 1980, Donelan et al, 1985, Fadaeiazar et al., 2020). The directional  
74 distribution and integrated values such as the mean wave direction are crucial parameters  
75 affecting wave growth through wind input, as the atmosphere forces energy into wave  
76 components that are aligned (and almost aligned) with wind. Despite their role, however,  
77 directional properties remain one of the less known properties of the ocean surface.  
78 Contemporary wave models use parametrizations to shape the directional spreading during the  
79 wave growth, which assume the directional distribution being unimodal (i.e. energy is  
80 concentrated around one dominant direction, Hasselmann et al. 1980, Mitsuyasu et al. 1975,  
81 Donelan et al. 1985) and defined by a directional spreading function of the form  $\cos^{2s}(\vartheta)$ , where  
82  $\vartheta$  is the wave propagation direction. Nevertheless, there is no general consensus on the shape of  
83 the directional distribution. Moreover, field and laboratory observations have also suggested that  
84 the nonlinear interactions induce a bimodal directional distribution in the early state of wave  
85 growth (Young 1995, Ewans 1998, Toffoli et al. 2010, Toffoli et al. 2017), with the angle of  
86 separation among peaks depending on the wave age and wind direction (Long and Resio 2006).  
87 Peaks eventually merge into a unimodal directional function consistent with  $\cos^{2s}(\vartheta)$  when  
88 approaching full development (e.g. Toffoli et al. 2017, Fadaeiazar et al., 2020).

89 Uncertainties on the directional properties affect the identification of those wave components  
90 that are aligned with the wind and thus translate into errors in the estimation of the wind input  
91 process in the wave prediction model. The extent of these errors is yet to be quantified. As  
92 contemporary satellite products cannot optimize wind sea, the latter remains a notable source of  
93 model errors, resulting in an overestimation of significant wave height (positive bias). This is  
94 exacerbated in the Southern Ocean (Ziegler et al. 2015)-a region covering an uninterrupted band  
95 of water around Antarctica south of the main landmasses of Africa, Australia, and South  
96 America—that is dominated by strong westerly winds, which blows all-the-year-round with  
97 almost unlimited fetches and speed in excess of 13 m/s during summer months and 18 m/s during  
98 winter months (Young et al. 2020). These intense winds generate some of the fiercest waves on  
99 the planet with high percentiles of wave height exceeding 5 m during summer and 7 m during  
100 winter (e.g. Babanin et al. 2019, Barbariol et al. 2019, Letraon et al. 2019, Vichi et al. 2019,  
101 Young et al. 2020).

102 The newly launched Chinese-French Oceanography Satellite (CFOSAT) uses Surface Wave  
103 Investigation Measurements (SWIM) sensor (Hauser et al. 2018) to monitor the ocean surface.  
104 Compared to SAR, SWIM resolves a broader range of wavelengths, spanning from 70 to 500 m,  
105 and returns a directional wave energy spectrum that includes both wind sea and swells. Here we  
106 discuss the effect of data assimilation on model performance in the Southern Ocean. We  
107 demonstrate that assimilating directional properties from SWIM spectra improves prediction of  
108 energy transfer during wave growth and concurrently of significant wave height. We show that

109 model bias is reduced more efficiently when compared with classical assimilation procedures  
110 that incorporate information on the significant wave height only.

## 111 **2 CFOSAT mission and SWIM spectra**

112 The instrument SWIM of CFOSAT is a real aperture scanning radar which provides directional  
113 wave spectra from several off-nadir beams (pointing at 6, 8 and 10°). Each spectrum is  
114 representative of an area of about  $\pm 35$  km along-track by 90 km on each side of the nadir track,  
115 and is discretised over 32 wave numbers from [0.0126–0.279] rad/m, corresponding to the  
116 wavelength domain [22–500] m, with a geometric progression of 1.1, and 12 directions, i.e.,  
117 every 15° with a 180° ambiguity in the propagation direction. During the calibration/validation  
118 phase of the mission a detailed analysis was carried out to evaluate the ability of SWIM to  
119 provide accurate parameters from the wave spectra (see Hauser et al. 2020) such as the dominant  
120 direction, dominant wave height and significant wave height. It was concluded that, except when  
121 waves propagate close to the along-track direction directional wave spectra can be provided with  
122 good accuracy over the wavelengths range of 70 to 500 m (see Hauser et al. 2020). In this study  
123 we use the directional wave spectra from the beam 10° which have been shown to perform better  
124 in comparison with the other beams (see Hauser et al, 2020). SWIM also provides Significant  
125 Wave Height (SWH) along its track from nadir measurements just like the classical altimeter  
126 measurement (referred to as SWIM-nadir). For the assimilation, we used observations made over  
127 a 36 days period from April 26 to 1 June 2019. During this period, 343885 wave spectra from  
128 SWIM were collected for the global ocean, and 95281 of which were from the Southern Ocean.

## 129 **3 Numerical model and data assimilation technique**

130 The MFWAM wave model describes the evolution of wave spectra in space and time  
131 through the wave action conservation equation with source terms representing the wave  
132 generation by the wind, the non-linear interactions and the wave breaking at sea surface. The  
133 wave model MFWAM of Meteo-France is based on the IFS-ECWAM computing code of the  
134 ECMWF (see IFS-38R2). The model MFWAM uses an ST4 dissipation term related to wave  
135 breaking as developed by Ardhuin et al. (2010). Also, in the MFWAM model the wind input  
136 source term takes into account a dissipation term due to the damping of the swell by the surface  
137 friction. The non-linear interactions are represented by the Discrete Interaction Approximation  
138 (DIA) which is a common approximation in numerical wave models due to its computational  
139 efficiency. The MFWAM model is used for the global wave system of the Copernicus Marine  
140 Service with a recent update which takes into account a spectra tail in the form of the Phillips'  
141 spectrum. This parameterization is important for the calculation of the total stress provided to the  
142 ocean model and the impact of waves on the atmosphere in a coupled simulation.

143 In the present study the model MFWAM uses a discretization of the wave spectrum in 24  
144 directions (from 0 to 360°) and 30 frequencies increasing from 0.035Hz with a geometric  
145 progression of 1.1. The MFWAM model is set for a global configuration with a grid resolution of  
146 0.5°. The model is forced by analyzed winds and sea ice fraction provided by the IFS  
147 atmospheric system of the ECMWF. Four sets of simulations were run : (i) with assimilation of  
148 wavenumber components  $K_x$  and  $K_y$  from SWIM spectra (run A); (ii) with assimilation of  
149 SWIM SWH only (run B); (iii) with assimilation of both SWH and wave number components

150 (run C); and (iv) without assimilation (run D) as a control run to examine the impact (or to build  
151 a benchmark database).

152 Wavenumber components were assimilated into the model with the following scheme  
153 (Aouf et al., 2006 & 2019): (i) model and SWIM spectra are partitioned to separate wind sea  
154 from swell systems, following Gerling (1992); (ii) partitions of the model spectra are matched  
155 with the SWIM counterpart; (iii) an optimal interpolation between model and observations to the  
156 two components  $K_x$  and  $K_y$  of the partition wave number is applied; and (iv) analyzed partitions  
157 are superposed to reconstruct the analyzed wave spectrum, with smoothing procedure to avoid  
158 gaps between partitions. Only modes with wavelengths greater than 70 m were used for the  
159 assimilation, while the first guess wave spectrum from the model stays unchanged otherwise.

160 The assimilation of SWH from SWIM instrument at nadir look consists in performing only the  
161 optimal interpolation scheme for SWH (as a stand-alone procedure or in conjunction with the  
162 assimilation of wavenumber components). Note, however, that assimilation of SWH further  
163 requires a scaling of the wave spectrum in the frequency range by using the empirical power  
164 laws developed in Lionello et al. (1992). This is the classical approach as used in most  
165 operational models (see Aouf and Lefevre 2015).

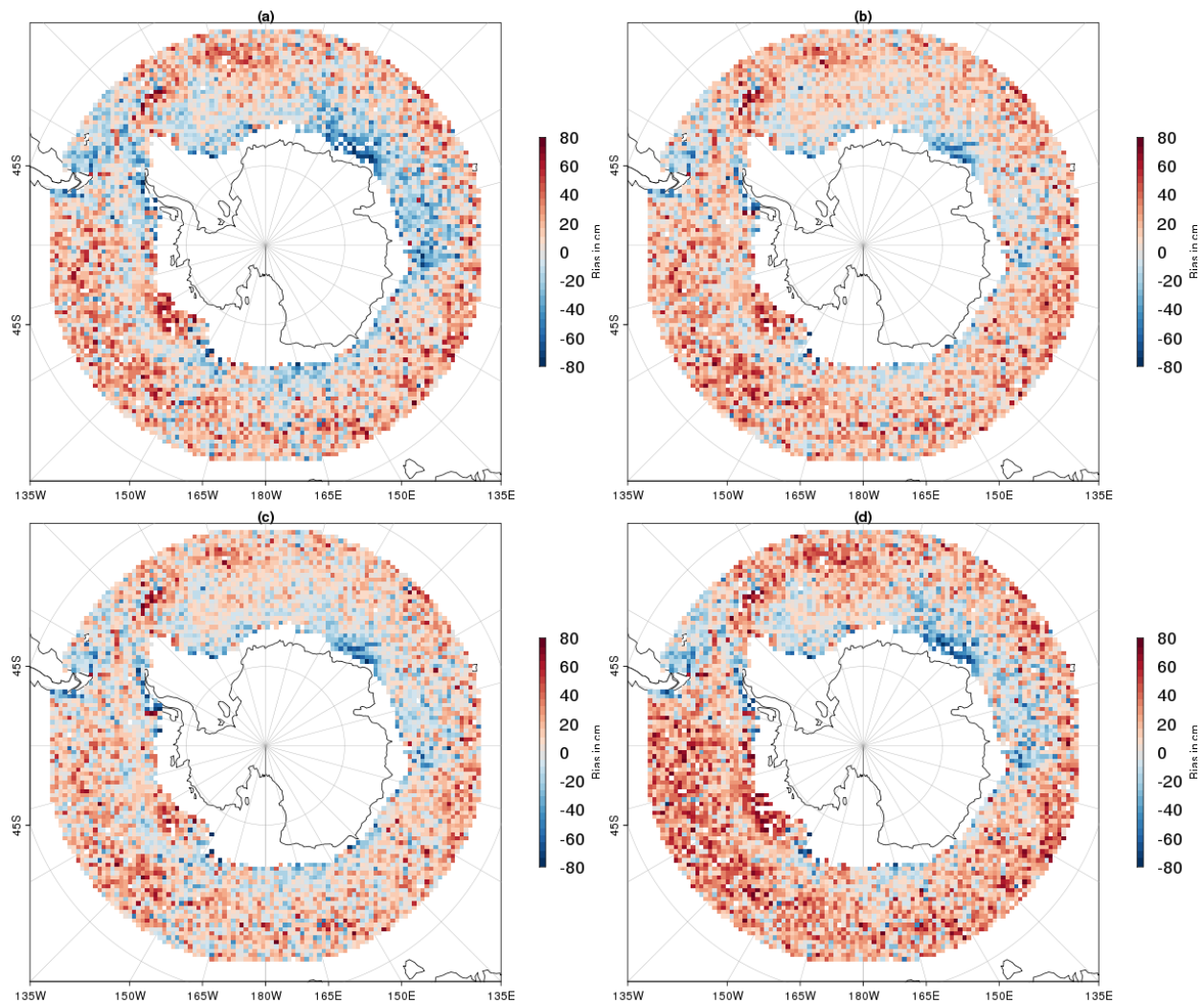
166 The study area focuses on the Southern Ocean where a large number of storm events with strong  
167 winds are generated during the Southern winter. We should remark that during the period of  
168 study surface wind speed exceeding 20 m/s represent 30% for the Pacific Southern Ocean  
169 between the longitudes 150°E-250°E.

170 The Southern Ocean is well covered by altimeter missions. Therefore, the validation of  
171 the model simulations is based on significant wave heights provided by the Jason-3, Saral/Altika  
172 and Sentinel-3 altimetry missions in this region. Super-observations of SWH from altimeters  
173 have been generated on the grid size of the model, which is  $0.5^\circ \times 0.5^\circ$ . Thus, to evaluate the  
174 impact of assimilation, we compare SWH from the four model runs with those provided by the  
175 altimeters on this grid size.  
176

### 177 **3 Results and discussions**

178 Biases on SWH from the model runs, with respect to the independent altimeter data, are  
179 presented in Fig.1 as maps covering the [50°S -70°S] area. For all runs, we can clearly see a  
180 dominant trend of positive bias in the Southern Ocean and the highest values are often found in  
181 the Pacific Southern Ocean. However negative bias of SWH are also observed in the Atlantic and  
182 Indian ocean near the Marginal Ice Zone (MIZ), where it is expected a strong uncertainty on  
183 local winds related to sea-ice melt-water. There is an evident reduction of bias when assimilating  
184 satellite data into the model. On average, the control run (without assimilation) leads to a mean  
185 bias for SWH of approximately 0.13 m (Fig. 1d) with maximum values reaching 1 m. The mean  
186 bias reduces to 0.10 m when assimilating the SWH (Fig. 1b). Incorporating wavenumbers in the  
187 assimilation contributes significantly to reduce the bias, the latter dropping to 0.03 m for  
188 assimilation of wavenumbers only (Fig. 1c) and 0.05 m, when assimilating both wavenumbers  
189 and SWH (Fig. 1c).

190 To examine the impact of the assimilation on high SWH in Southern Ocean, scatter analysis of  
191 SWH from MFWAM versus the one from altimeter sensors have been performed for SWH  
192 greater than 5 m. Overall, run A results in an excellent correlation with altimeter data, with  
193 scatter diagram laying on the slope 1:1 and intercept of 0.04m, substantiating the significant bias  
194 reduction. On the contrary, run B shows an overestimation of model results, with data point  
195 distributing along a slope of 1.05 and intercept of -0.19m and a mean positive bias of 0.13 m. In  
196 terms of Normalized Root Mean Square Error (NRMSE), the best performance for high SWH  
197 (greater than 5m) is obtained when assimilating wavenumber components (runs A and C) with  
198 10.3%. While for the assimilation of SWH only and the control run, NRMSE are roughly 10.6%  
199 and 11%, respectively.

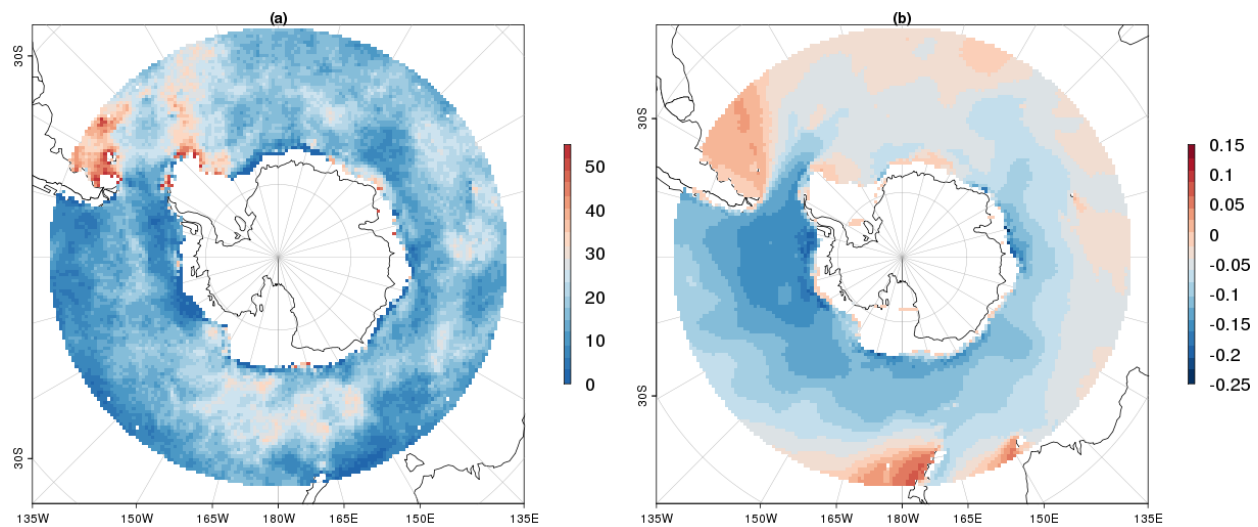


200  
201 **Figure 1.** Bias maps of SWH (in cm) for simulations of the MFWAM model in comparison with  
202 altimeters Jason-3, Saral/Altika and Sentinel-3 during the period starting from 26 April to 1 June  
203 2019. (a), (b), (c) and (d) indicate runs A, B, C and C, respectively.

204 To explain this finding, it is interesting to note that in the wind wave growth phase there is a  
205 transfer of wave energy from the high frequencies to the smaller frequencies until an equilibrium

206 state is reached. In general the wind input term in a wave model which describes the wave  
207 growth depends, for each frequency, upon the difference of wave and wind directions. The fact  
208 that the assimilation of wavenumber components corrects the wave direction and the dominant  
209 frequency leads directly to an improvement of the wave growth and the energy transfer for wind  
210 waves before the equilibrium state.

211 Recall that the wave age which is expressed as the ratio of peak wave phase speed  $C_p$  and the  
212 surface wind speed  $U_{10}$ , indicates whether the sea state is windsea or swell dominant. The  
213 windsea can therefore be identified by a wave age  $C_p/U_{10}$  lower than 1. Figure 2a shows the  
214 regional distribution of wind sea, by the probability of occurrence associated with a wave age  
215 smaller than 1 (estimated over the analyzed period). There is a general predominance of wind sea  
216 throughout the entire Atlantic Ocean and Indian Ocean sectors. This is due to the occurrence of  
217 relatively close storm systems, which limits fetch for wave growth.



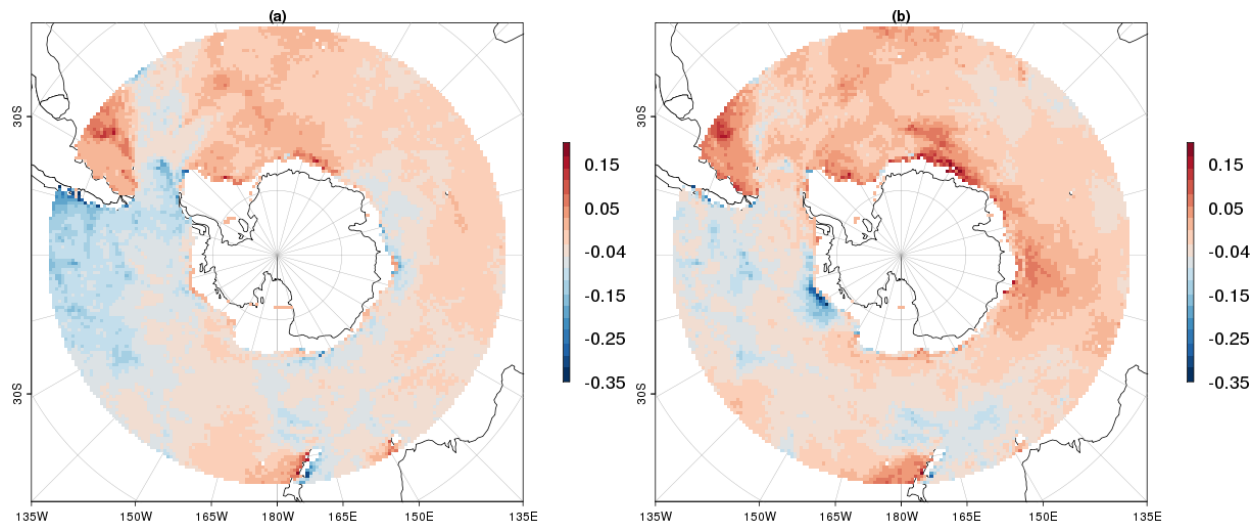
218  
219 **Figure 2.** (a) Probability of occurrence (color code) of dominant windsea sea state  
220 ( $C_p/U_{10} < 1$ ) from the control run A. (b) mean difference of SWH between run A and run D during  
221 the period from 26 April to 1 June 2019.

222 The Pacific Ocean sector, on the contrary, shows two distinct occurrence zones. The first  
223 zone is an extended area between  $150^\circ\text{E}$ - $150^\circ\text{W}$  and South of New Zealand representing a strong  
224 occurrence (greater than 25%) of wind sea with uninterrupted fetch conditions. Elsewhere of this  
225 zone the low probability of wind sea (i.e. predominance of swell) indicate the presence of fully-  
226 developed waves of swell, for instance the drake passage and Chile sector. Figure 2b shows the  
227 difference between the mean SWH derived from model runs with assimilation of partition  
228 wavenumber components (run A) and benchmark simulation (run D). The assimilation results in  
229 a significant reduction of the significant wave height throughout the Southern Ocean in  
230 comparison with the control run. The extent of this difference depends on the wave age (cf.  
231 Figure 2a). Small differences are reported in the Atlantic Ocean and Indian Ocean Sector, where  
232 swell is not dominant (cf. Fig. 2a), while the largest average differences—up to  $-0.25$  m—are  
233 found in the Pacific Ocean sector, especially in the Amundsen Sea and Bellingshausen Sea



234 subsectors and in the Drake passage. There are the areas where the wind sea generated South of  
235 New Zealand has transformed into a swell after a long, uninterrupted propagation.

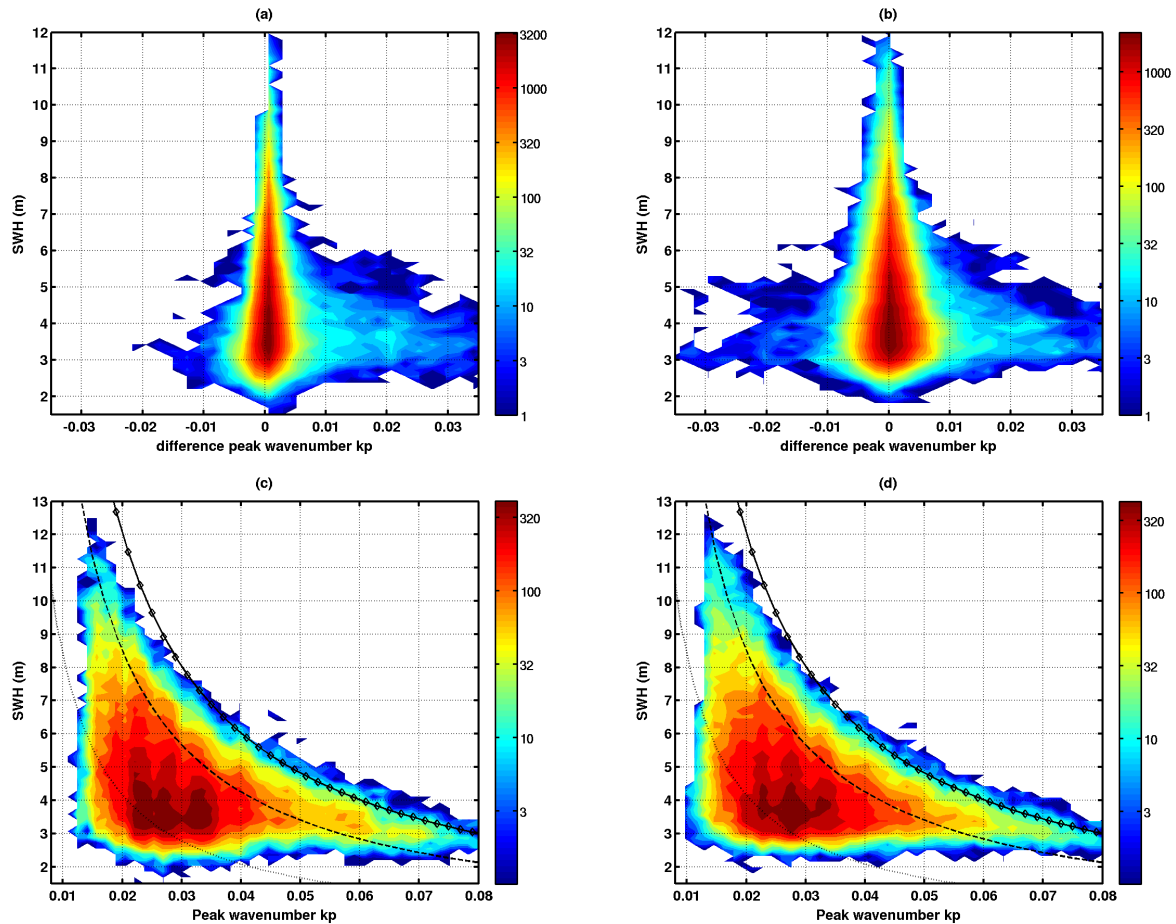
236 Let's call the difference between assimilation runs and the control run the analysis  
237 increment. The impact of run A on the peak wave age indicates two trends on the analysis  
238 increment as shown in Figure 3a. The first trend concerns the Pacific Ocean sector and Drake  
239 Passage where there is a strong negative analysis increment on average which is linked to the  
240 overestimation of the wave age by the run D. The average difference in this sector reaches -0.25.  
241 The second trend is observed in the Atlantic and Indian oceans sectors where we see that the  
242 assimilation of partitions wavenumbers induces a positive increment. This latter indicates an  
243 underestimation of the wave age by the control run D with a maximum average difference of  
244 0.15. By comparing figures 3a and 3b we see that run B mainly indicates positive increments in  
245 all sectors and enhanced in some regions the impact in comparison with run A. The negative  
246 increment caused by run B is limited and not significant correction. This can be explained by the  
247 use of empirical power laws (Lionello et al. 1992) which seems less efficient to correct peak  
248 wave age in unlimited fetch conditions in Pacific Southern Ocean.



249  
250 **Figure 3.** Average of difference of wave age ( $C_p/U_{10}$ ) of runs with and without assimilation  
251 during the period between 26 April and 1 June 2019. (a) stand for the assimilation of  
252 wavenumber components (run A), while (b) indicate the assimilation of SWH only. Negative  
253 values mean overestimation of wave age and conversely positive values indicate underestimation  
254 of the control run.

255 To investigate the difference between run A and run B we analyzed the analysis  
256 increment of dominant wavenumbers from these two runs in comparison with the control run D.  
257 Figure 4a and 4b show respectively the analysis increment of the dominant wavenumber of runs  
258 A and B as a function of SWH located on the altimeters tracks used for the bias evaluation in the  
259 Southern Ocean. We can clearly see that the assimilation of the partition wavenumbers mainly  
260 leads to a positive correction of the dominant wavenumber  $k_p$  (Fig.4a), which indicates an  
261 underestimation of the control run D. This increase of the wave number is clearly visible for  
262 strong SWH (greater than 5 m), which shows that assimilation maintains the wave regime in the

263 growth phase. Figure 4c reveals that the majority of the dominant wavenumbers  $k_p$  points are  
 264 between the theoretical curves of young and mature seas as given by the Elfouhaily spectrum  
 265 (Elfouhaily et al., 1997). Figure 4c clearly indicates a good consistency of the variation of  
 266 dominant wavenumber with SWH in comparison with theoretical curves. On the contrary for  
 267 run B (Fig. 4b), we notice that the correction of  $k_p$  is dominated by negative analysis increments  
 268 for strong SWH (greater than 5 m). This explains the difficulty of run B to reduce the bias for  
 269 large SWH, and also to improve the dominant wavenumbers during the growth phase. Figure 4d  
 270 also indicates that the number of  $k_p$  points between the young and mature sea curves is smaller  
 271 compared to Figure 4c.



272

273 **Figure 4.**(a,b): variation of analysis increment of peak wavenumber with SWH, for model runs  
 274 A and B, respectively. (c,d): Relation between SWH peak wavenumber with, for model runs A  
 275 and B., respectively. The dotted, dashed and diamond lines indicate the theoretical variation for  
 276 peak wavenumber of young (wave age=0.7), mature (wave age=1) and fully developed (wave  
 277 age=1.2) seas according to the wave spectrum model of Elfouhaily et al. (1997). With equations  
 278 (37) and (38) in Elfouhaily et al.(1997), we obtained the following relation  $SWH=(0.17/k_p)*\Omega^{-1.7}$   
 279 where  $\Omega$  is the inverse wave age. Color bars indicate the density of points by pixel.

## 280 **4 Conclusions**

281 The Southern Ocean is dominated by strong wave systems which can impact air-sea  
282 interaction and ocean and sea-ice dynamics (e.g. Humphries et al. 2016; Schamle et al. 2019,  
283 Thurnherr et al. 2020, Vichi et al. 2019, Alberello et al. 2020). Contemporary wave models  
284 provide biased estimates of the significant wave height in this region, despite assimilation of  
285 satellite observations. These, however, are limited to significant wave height or truncated  
286 directional wave energy spectra, which account for swell systems, but neglect the short wave  
287 components of the wind sea. However, with the instrument SWIM carried by the CFOSAT  
288 satellite, it is now possible to detect directional wave spectra that resolve both swell and wind-  
289 wave systems. This study has demonstrated that the assimilation of the wavenumber components  
290 from more comprehensive spectra enhance model prediction of energy transfer during the wave  
291 growth phase and concurrently improve estimation of the significant wave height in the Southern  
292 Ocean. A validation was conducted by comparing significant wave height from model runs with  
293 and without assimilation against observations from altimeter sensors. Overall, data assimilation  
294 reduces biases. Model runs, however, show that assimilation of wavenumber components (i.e.  
295 directional properties) is more efficient in optimizing the model and results in more substantial  
296 bias reduction (from 13cm bias without assimilation to 3cm with assimilation) than assimilation  
297 of significant wave height only.

298 Furthermore, the results show that the assimilation of the wavenumbers components  
299 corrects significantly the wave age and the dominant wavenumber in the Southern Ocean, which  
300 keeps the wind waves between young and mature seas regimes. This has been verified with the  
301 theoretical growth curves (SWH as function with  $k_p$ ) as given by Elfouhaily et al. (1997). We  
302 have observed a better spread of the impact on wave age when using directional observations  
303 around the Southern Ocean in comparison with the assimilation of significant wave height only.  
304 The transition to swell regime and the propagation in northern ocean region is also well tracked  
305 as it is observed in Pacific Southern Ocean. However, the assimilation of SWH only showed a  
306 limited and localized impact on the wave age.

307 This research opens perspectives on the use of the directional properties of SWIM  
308 instrument of CFOSAT mission to improve wave model and also provide accurate wave spectra.  
309 We expect a promising use of the assimilation of wave number components for ocean/waves  
310 coupling in terms of momentum flux transfer in southern ocean where gas exchanges are still  
311 poorly understood in climate models.

## 312 **Acknowledgments and data**

313 This work is funded by the French Space Agency CNES in the frame of TOSCA national  
314 program. The level 2 data used here are processed by SWIM algorithms version V5.0.1. The data  
315 are available and open access on <ftp-access.aviso.altimetry.fr>. The authors would also like to  
316 thank Alice Dalphinnet and Malek Ghantous for helping to the preparation of the manuscript.  
317

318 **References**

- 319 Alberello, A., Bennetts, L., Heil, P., Eayrs, C., Vichi, M., MacHutchon, K., Onorato, M. &  
320 Toffoli, A.: Drift of Pancake Ice Floes in the Winter Antarctic Marginal Ice Zone During Polar  
321 Cyclones, *Journal of Geophysical Research: Oceans*, 125, e2019JC015 418,  
322 doi.org/10.1029/2019JC015418, 2020.
- 323 Aouf L., Dalphinet, A., Hauser, D., Delaye, L., Tison, C., Chapron, B., Hermozo, L., &Tourain,  
324 C. (2019), On the Assimilation of CFOSAT Wave Data in the Wave Model MFWAM :  
325 Verification Phase, proceedings of IGARSS 2019 - IEEE International Geoscience and Remote  
326 Sensing Symposium, Yokohama, Japan, 2019, pp. 7959-7961, doi:  
327 10.1109/IGARSS.2019.8900180.
- 328 Aouf L. & Lefèvre J-M. (2015), On the impact of the assimilation of SARAL/Altika wave data  
329 in the operational wave model MFWAM, *Marine Geodesy*, 38, 381-395.  
330 doi:10.1080/01490419.2014.1001050
- 331 Aouf, L., Lefèvre, J-M. & Hauser D. (2006), Assimilation of directional wave spectra in the  
332 wave modelWAM: An impact study from synthetic observations in preparation for the  
333 SWIMSAT Satellite mission. *J Atmos Ocean Technol.* doi: 10.1175/JTECH1861.1
- 334 Ardhuin, F., Rogers, E., Babanin, A., Filippot, J-F., Magne, R., Roland, A., Van Der  
335 Westhuysen, A.; Queffeuilou, P., Lefèvre, J-M., Aouf, L. & Collard, F. (2010), Semi empirical  
336 Dissipation Source Functions for Ocean Waves. Part I: Definition, Calibration, and Validation. *J.*  
337 *Phys. Oceanogr.*, **40**, 1917–1941, doi:10.1175/2010JPO4324.1.
- 338 Babanin A. V., Rogers, E. W., de Camargo, R., Doble, M., Durrant, T., Filchuk, K., Ewans, K.,  
339 Hemer, M., Janssen, T., Kelly-Gerreyn, B., Machutchon, K., McComb, P., Qiao, F., Schulz, E.,  
340 Skvortsov, A., Thomson, J., Vichi, M., Violante-Carvalho, N., Wang, D., Waseda, T., Williams,  
341 G. &Young, I. R. (2019) Waves and swells in high wind and extreme fetches, measurements in  
342 the Southern Ocean, *Frontiers in Marine Science*, 6, 361, DOI:10.3389/fmars.2019.00361
- 343 Barbariol, F., Benetazzo, A., Bertotti, L., Cavaleri, L., Durrant, T., McComb, P., & Sclavo, M.:  
344 Large waves and drifting buoys in theSouthern Ocean, *Ocean Engineering*, 172, 817–828, 2019
- 345 Csanady, G. T.: Air-sea interaction: laws and mechanisms, Cambridge University Press, 2001.
- 346 Collard F., Ardhuin, F. &Chapron, B. :Monitoring and analysis of ocean swell fields from space  
347 : New methods for routines observations, *Journal of Geophysical Research*,  
348 10.1029/2008JC005215, 14, issue C7, 2005
- 349 ECMWF (2013) Part VII : IFS Documentation CY38R1, Part VII ECMWF Wave Model.  
350 <https://www.ecmwf.int/node/9248>
- 351 Ewans K., 1998, Observations of the directional wave spectrum of fetch-limited waves, *J. Phys.*  
352 *Oceanogr.*, **28**, 498–512.
- 353 Donelan, M. A., Hamilton, J. &Hui, W. H. (1985) : Directional spectra of wind-generated waves.  
354 *Philos. Trans. Roy. Soc. London.*, **A315**, 509–562.
- 355 Elfouhaily, T., Chapron, B., Katsaros, C. &Vandemark, D. :A unified directional spectrum for  
356 long and short wind-driven waves. *Journal of Geophysical Research*, Volume 102, C7,  
357 <https://doi.org/10.1029/97JC00467>.
- 358 Fadaeiazar, E., Leontini, J., Onorato, M., Waseda, T., Alberello, A.& Toffoli, A.: Fourier  
359 amplitude distribution and intermittency in mechanically generated surface gravity waves, *Phys.*  
360 *Rev. E*, 102, 013 106, doi.org/10.1103/PhysRevE.102.013106, 2020

- 361 Humphries, R. S., Klekociuk, A. R., Schofield, R., Keywood, M., Ward, J. & Wilson, S. R.:  
362 Unexpectedly high ultrafine aerosol concentrations above East Antarctic sea ice, *Atmos.*  
363 *Chem. Phys.*, 16, 2185–2206, doi.org/10.5194/acp-16-2185-2016, 2016.
- 364 Gerling, T. W., Partitioning sequences and arrays of directional ocean wave spectra into  
365 component wave systems, *J. Atmos. Oceanic Technol.*, 9, 444–458, 1992.
- 366 Hasselmann K., P. T. Barnett, E. Bouws, H. Carlson, E. D. Cartwright, K. Enke, A. J. Ewing, H.  
367 Gienapp, E. D. Hasselmann, P. Kruseman, A. Meerburg, P. Muller, D. Olbers, K. Richter, W.  
368 Sell, & H. Walden. Measurements of wind-wave growth and swell decay during the joint north  
369 sea wave project (jonswap). *Deut. Hydrogr. Z.*, 8 :1–95, 01 1973.
- 370 Hasselmann, D. E. & Dunckel, M. & Ewing, J. A. (1980) : Directional wave spectra observed  
371 during JONSWAP 1973. *J. Phys. Oceanogr.*, **10**, 1264–1280.
- 372 Hasselmann K., Chapron B., Aouf L., Ardhuin F., Collard F., Engen G., Heimbach P., Janssen  
373 P., Krogstad H., Lehner S., Li J-G., Li Xiaoming, Rosenthal W. & Schulz-Stellenfleth J. (2012) :  
374 The ERS SAR Wave Mode – A Breakthrough in global ocean wave observations. European  
375 Space Agency, (Special Publication) ESA SP. 1326.
- 376 Hauser D., et al., "New Observations From the SWIM Radar On-Board CFOSAT: Instrument  
377 Validation and Ocean Wave Measurement Assessment," in *IEEE Transactions on Geoscience*  
378 *and Remote Sensing*, doi: 10.1109/TGRS.2020.2994372.
- 379 Kuik, A. J., van Vledder, G. Ph. & L. H. Holthuisen, (1988): A method for the routine analysis of  
380 pitch-and-roll buoy wave data. *J. Phys. Oceanogr.*, **18**, 1020–1034.
- 381 Le Traon P. Y., Reppucci A. & Alvarez Fanjul E. et al (2019) From Observation to Information  
382 and Users: The Copernicus Marine Service Perspective. *Front Mar Sci.* doi:  
383 10.3389/fmars.2019.00234
- 384 Lionello, P., Gunther, H. & Janssen, P. A. E. M. (1992). Assimilation of altimeter data in a  
385 global third generation wave model. *J. Geophys. Res.*, C97, 14453–14474.
- 386 Long, C. E. & Resio, D. (2007). Wind wave spectral observations in Currituck Sound, North  
387 Carolina. *J. Geophys. Res.* 112, CO5001.
- 388 Mitsuyasu, H., Tasai, F., Suhara, T., Mizuno, S., Ohkusu, M., Honda, T. & Rikiishi, K. & (1975).  
389 Observations of the directional spectrum of ocean waves using a clover leaf buoy. *J. Phys.*  
390 *Oceanogr.* 5, 750–760.
- 391 Pierson, W. J., & Moskowitz, L., A proposed spectral form for fully developed wind sea based  
392 on the similarity theory of S. A. Kitaigorodskii, *J. Geophys. Res.*, 69, 5181–5190, 1964.
- 393 Phillips, O. M., *The Dynamics of the Upper Ocean*, 2nd ed., Cambridge Univ. Press, New York,  
394 1977.
- 395 Resio D. T., Linwood V. & Ardag D., Characteristics of directional wave spectra and  
396 implications for detailed-balance wave modeling, *Ocean Modelling*, doi:10.1016/j.ocemod.  
397 2015. 09.009
- 398 Schmale, J., Baccarini, A., Thurnherr, I., Henning, S., Efraim, A., Regayre, L., Bolas, C.,  
399 Hartmann, M., Welti, A., Lehtipalo, K., Aemisegger, F., Tatzelt, C., Landwehr, S., Modini, R. L.,  
400 Tummon, F., Johnson, J. S., Harris, N., Schnaiter, M., Toffoli, A., Derkani, M., Bukowiecki, N.,  
401 Stratmann, F., Dommen, J., Baltensperger, U., Wernli, H., Rosenfeld, D., Gysel-Ber, M. &  
402 Carslaw, K. S.: Overview of the Antarctic Circumnavigation Expedition: Study of Preindustrial-  
403 like Aerosols and Their Climate Effects (ACE-SPACE), *Bull. Am. Meteorol. Soc.*, 100, 2260–  
404 2283, doi.org/10.1175/BAMS-D-18-0187.1, 2019.
- 405 Thurnherr, I., Kozachek, A., Graf, P., Weng, Y., Bolshiyarov, D., Landwehr, S., Pfahl, S.,  
406 Schmale, J., Sodemann, H., Steen-Larsen, H. C., Toffoli, A., Wernli, H. & Aemisegger, F.:

407 Meridional and vertical variations of the water vapour isotopic composition in the marine  
408 boundary layer over the Atlantic and Southern Ocean, *Atmos. Chem. Phys.*, 20, 5811–5835,  
409 doi.org/10.5194/acp-20-5811-2020, 2020  
410 Toffoli, A., Proment, D., Salman, H., Monbaliu, J., Frascoli, F., Dafilis, M., Stramignoni, E.,  
411 Forza, R., Manfrin, M. & Onorato, M., 2017, Wind Generated Rogue Waves in an Annular  
412 Wave Flume, *Phys. Rev. Letters*, 118, issue 14, 10.1103/PhysRevLett.118.144503.  
413 Toffoli, A., Onorato, M., Bitner-Gregersen, E.M. & Monbaliu, J. (2010). Development of a  
414 bimodal structure in ocean wave spectra. *J. Geophys. Res.* 115.  
415 Vichi, M., Eayrs, C., Alberello, A., Bekker, A., Bennetts, L., Holland, D., de Jong, E., Joubert,  
416 W., MacHutchon, K., Messori, G., Mojica, J. F., Onorato, M., Saunders, C., Skatulla, S. &  
417 Toffoli, A.: Effects of an explosive polar cyclone crossing the Antarctic marginal ice zone,  
418 *Geophys. Res. Lett.*, 46, 5948–5958, 2019.  
419 Young, I. R. 1999: Seasonal variability of the global ocean wind and wave climate, *Int. J.*  
420 *Climatol.*, 19, 931-950, doi:10.1002/(SICI)1097-0088(199907)19:9<931  
421 Young, I. R., Fontaine, E., Liu, Q., & Babanin, A. V.: The Wave Climate of the Southern Ocean,  
422 *J. Phys. Oceanogr.*, 50, 1417–1433, 2020.  
423 Young I. R., Verhagen, L. A. & Banner, M. L. (1995) : A note on the bimodal directional  
424 spreading of fetch-limited wind waves. *J. Geophys. Res.*, 100 (C1), 773–778.  
425 Zieger, S., Babanin, A. V., Rogers, W. E. & Young, I. R.: Observation-based source terms in the  
426 third-generation wave model WAVE-WATCH, *Ocean Modelling*, 96, 2–25, 2015.

427

428

429

430

431